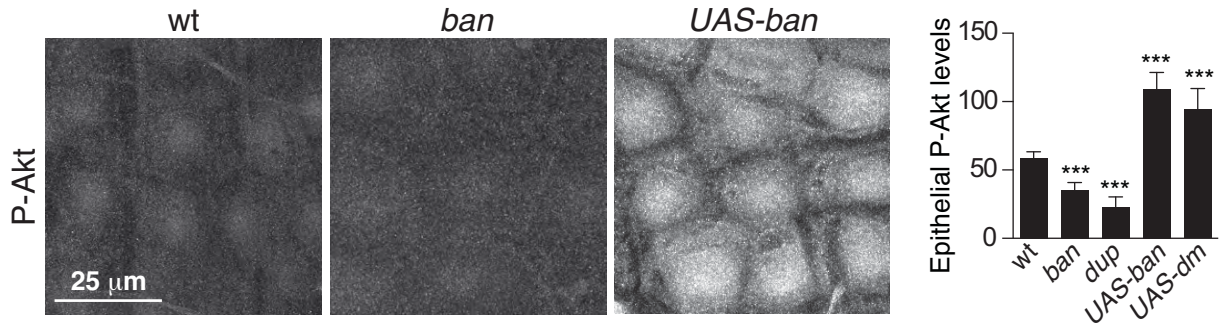

Figure S1. Phospho-Akt levels are responsive to *ban* activity and to endoreplication. Representative images of P-Akt staining in body wall epithelial cells of wild-type (wt), *ban* mutant, or epithelial *ban* overexpressing larvae are shown. Mean pixel intensity values for P-Akt staining. $n \geq 50$ cells for each genotype. Error bars represent standard deviation. ***$P<0.001$ compared to wt; one way ANOVA with a post-hoc Dunnett's test.

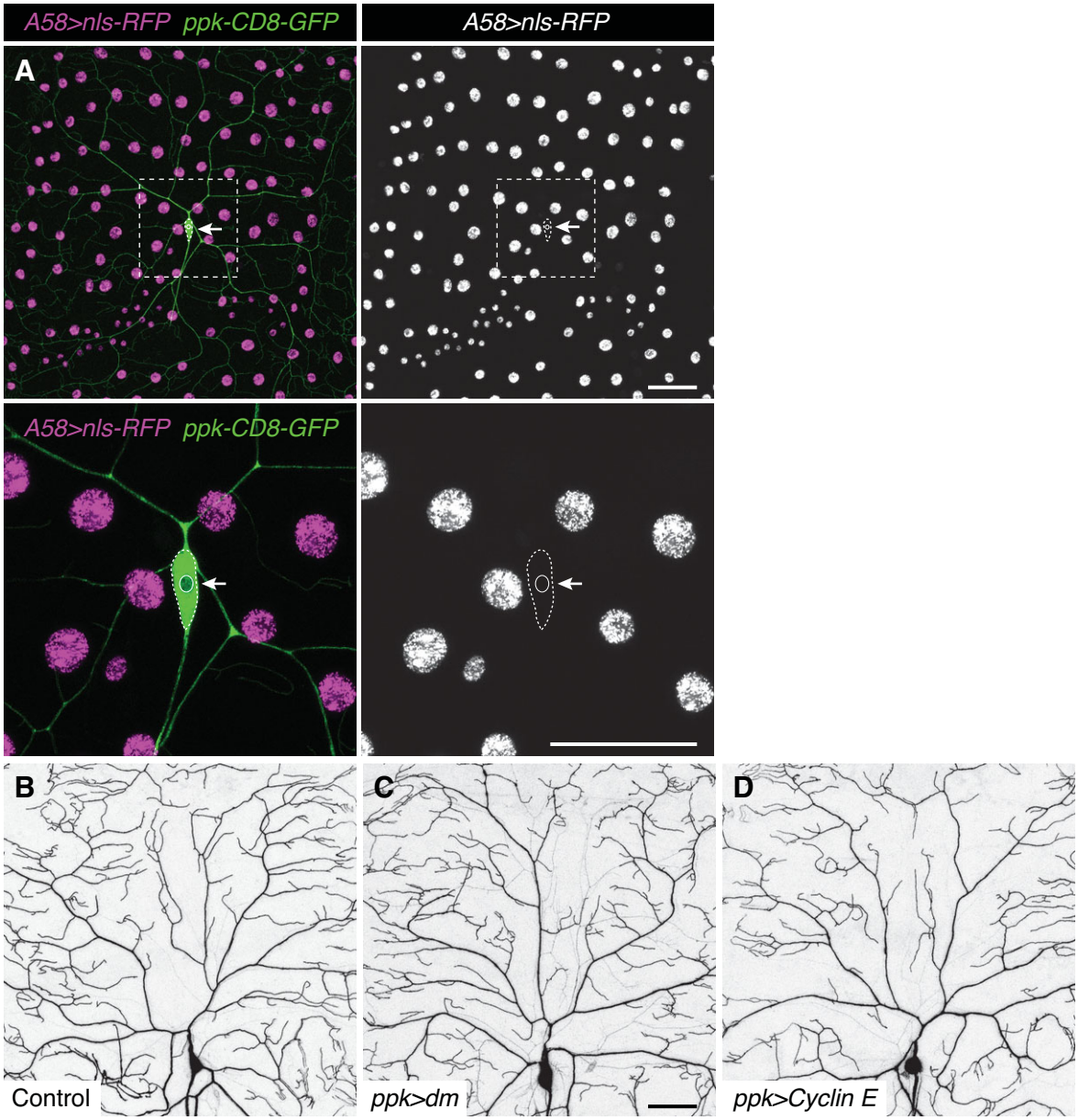

Figure S2. Epithelial specificity of *A58-Gal4* driver. (A) Larval *A58-Gal4* expression visualized by *UAS-nls-redStinger*. Although *A58-Gal4* is expressed throughout the epidermis, with the exception of apodemes, expression is not detectable in C4da neurons (arrow; labeled by *ppk-CD8-GFP*). (B-D) C4da dendrites in Control (*ppk-CD8-GFP, ppk-gal4* x w^{118}) larvae (B) or larvae overexpressing *UAS-dm* (C) or *UAS-Cyclin-E* in C4da neurons. Neuronal overexpression of endoreplication regulators does not alter C4da growth/patterning, demonstrating that dendrite growth defects caused by *A58*-driven expression of *UAS-dm* and *UAS-Cyclin-E* are not due to leaky neuronal expression of the driver. Scale bars, 50 μm.

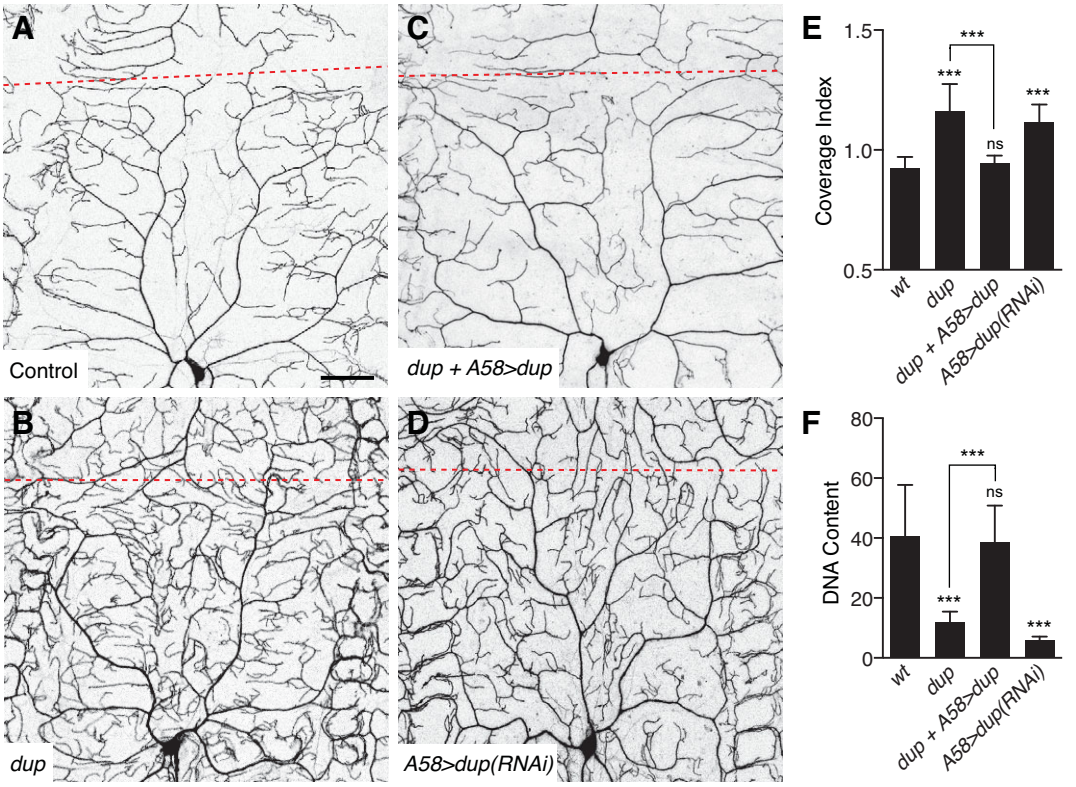

Figure S3. *dup* is required in epithelial cells to regulate epithelial ploidy and C4da dendrite growth. Compared to wt (A), blocking endoreplication with mutation in *dup* (B) increased dendrite growth and coverage. This dendrite overgrowth phenotype was completely rescued by resupplying *UAS-dup* to epithelial cells of homozygous dup mutant larvae (C). Epithelia-specific knockdown of *dup* (*A58>dupRNAi*) (D) caused dendrite defects comparable to dup mutation, demonstrating that dup is required in epithelial cells to support dendrite growth. (E) Quantification of dendrite coverage defects in the indicated genotypes. *n*=8 dendrites for each genotype. (F) *dup* is required in epithelial cells to support epithelial endoreplication. Quantification of DNA content in epithelial cells of the indicated genotype; measurements were as indicated in Fig. 2. *n*>20 cells for each genotype. Error bars represent standard deviation. **P*<0.05, ***P*<0.01, ***P*<0.001; ns, not significant; one-way ANOVA with a post-hoc Dunnett's test. Red dashed lines mark dorsal midline. Scale bars, 50 μm. Images in (A) and (B) are reproduced from Fig. 3.

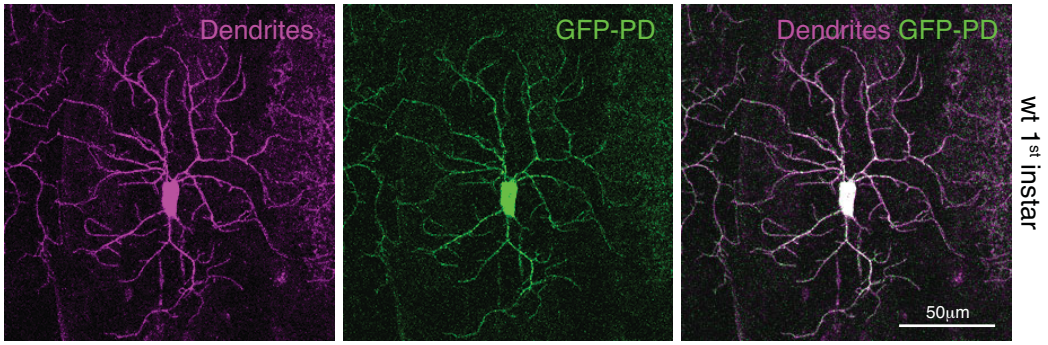

Figure S4. GFP-PD activity in first instar larvae.
Both halves of the proximity detector were expressed in C4da neurons (*ppk-gal4>UAS-sp1-10GFP* + *ppk-sp11GFP*) and GFP-PD activity was monitored in newly eclosed first instar larvae. Imaging settings were identical to those used in Figure 4.

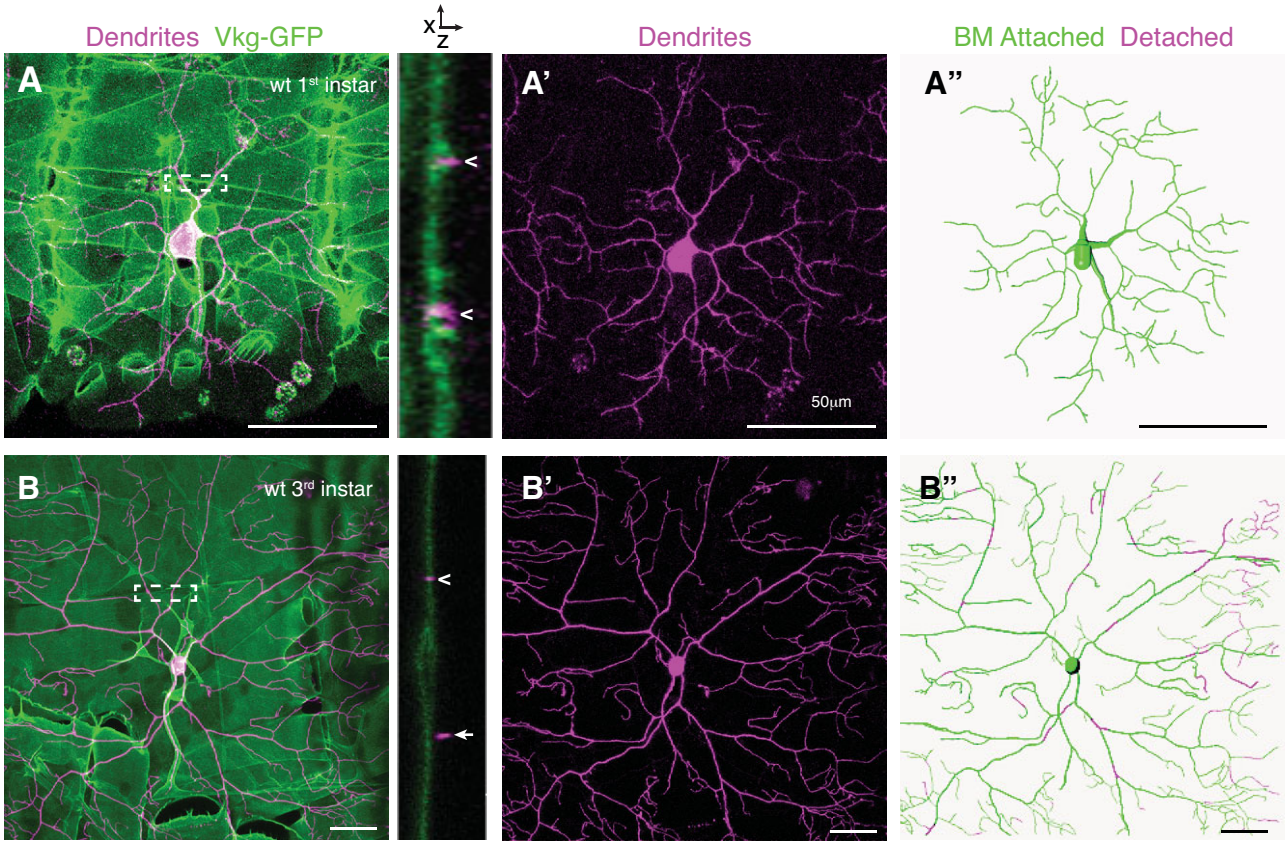

Figure S5. Live imaging of dendrites and the ECM using a neuronally-expressed membrane marker (*ppk-CD4-tdTomato*) and a GFP enhancer trap in *Drosophila viking* (*vkg-GFP*) to monitor dendrite-ECM colocalization. Representative maximum projections of 3D stacks captured by taking 200 nm optical sections are shown for wild type first instar larvae (A) and wild type third instar larvae (B). Orthogonal slices are shownfor the region marked by a white dashed box, and in the orthogonal slice attached dendrites are marked with carats (>) and detached dendrites are marked with asterisks (*). In the traces, dendrites that colocalize with Vkg-GFP are colored green whereas detached dendrites are colored magenta. Note the increase in dendrite detachment from the basement membrane in third instar larvae.

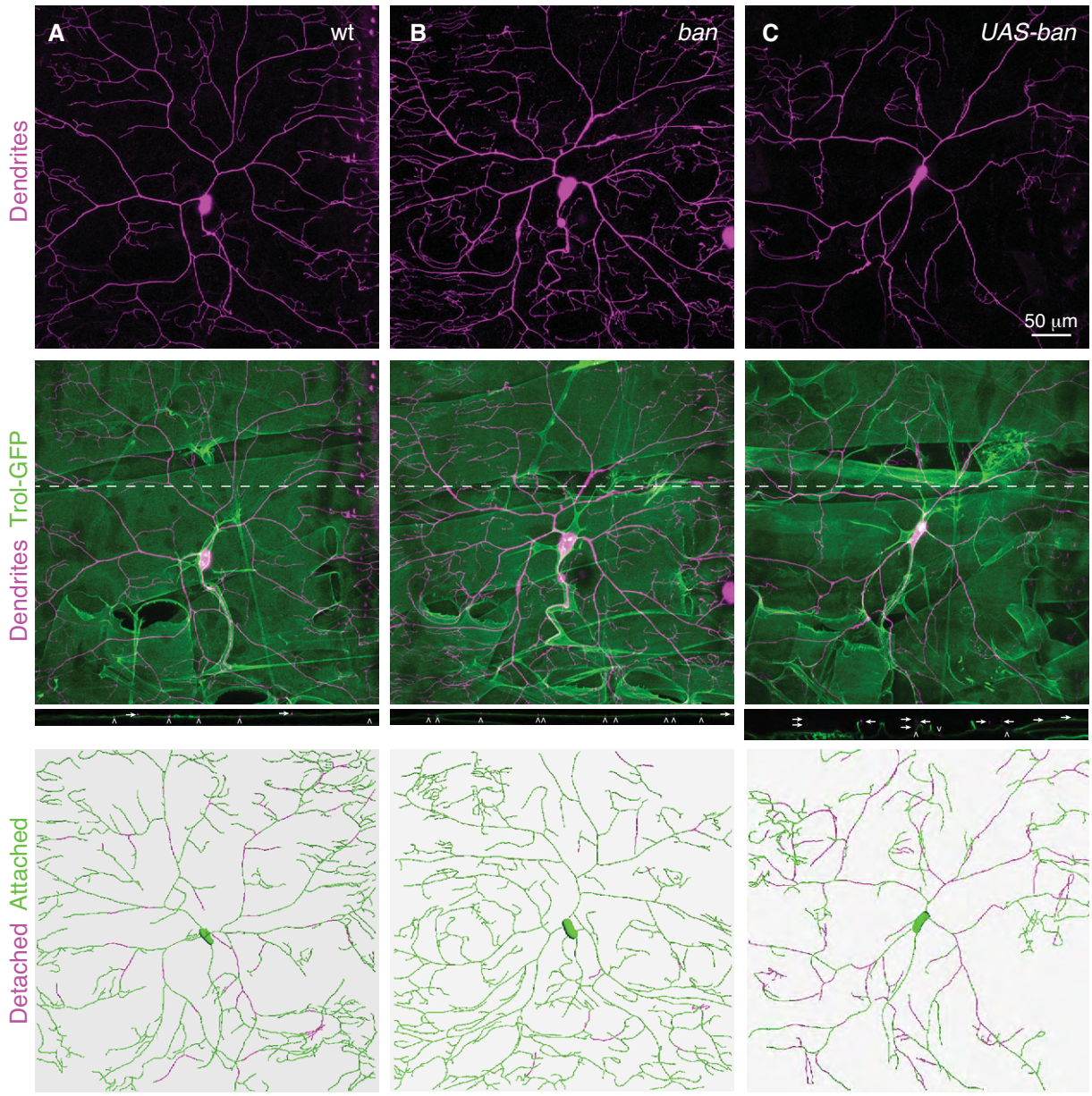

Figure S6. Live imaging of dendrites and the ECM using a neuronally-expressed membrane marker (*ppk-CD4-tdTomato*) and a GFP enhancer trap in the gene encoding *Drosophila* Perlecan (*trol-GFP*) to monitor dendrite-ECM colocalization in WT third instar larvae (A), *ban* mutant third instar larvae (B), and epithelial *ban* over-expressing instar larvae (C). 3D stacks were captured by taking 200 nm optical sections; maximum projections are shown. Following deconvolution, colocalization was measured between dendrites and Perlecan. Detached dendrites are marked with arrows in cross section and colored magenta in dendrite traces, whereas attached dendrites are marked with carets in cross section and colored green in dendrite traces.

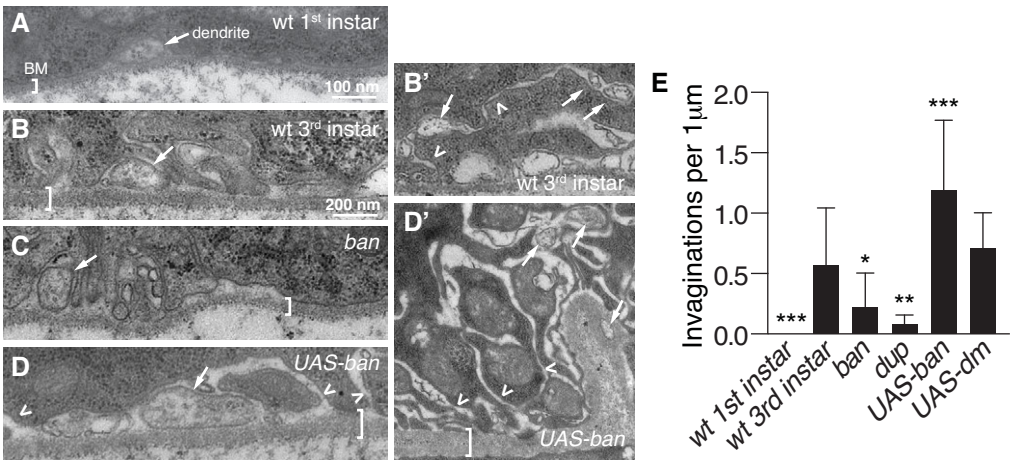

Figure S7. *ban* regulates epithelial internalization of dendrites. (A-D) TEM micrographs of the indicated genotypes. Dendrites (arrows) were identified as processes containing arrays of multiple parallel microtubules near the basal epithelial surface. Brackets mark BM; scale is identical in (B-D). (E) Epithelial basal plasma membrane invagination frequency was scored in 15 images (from multiple larvae) and the mean frequency of invaginations is plotted for the indicated genotypes. Other than wt first instar samples, all samples were from third instar larvae. Error bars represent standard deviation. **P*<0.05, ***P*<0.01, ****P*<0.001 compared to wt 3rd instar; one way ANOVA with a post-hoc Dunnett's test.

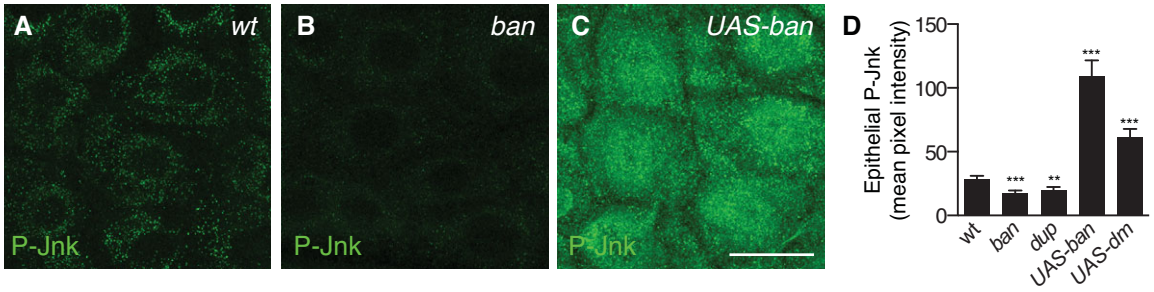

Figure S8. P-Jnk immunoreactivity in body wall epithelial cells is developmentally regulated by endoreplication. Representative images of P-Jnk staining in third instar body walls of wild-type (A), *ban* mutant (B), and epithelial *ban* overexpressing (C) larvae are shown. (D) Quantification of P-Jnk immunoreactivity for the indicated genotypes. Fillets of all genotypes were stained together with wild type fillets to ensure that staining conditions were comparable and all images were captured using identical settings. Means represent average pixel intensity of polygons outlining $n>50$ single cells (ImageJ). Error bars represent standard deviation. $^{**}P<0.01$, $^{***}P<0.001$; one way ANOVA compared to wild type with a post-hoc Dunnett's test. Scale bar, 25 μm.

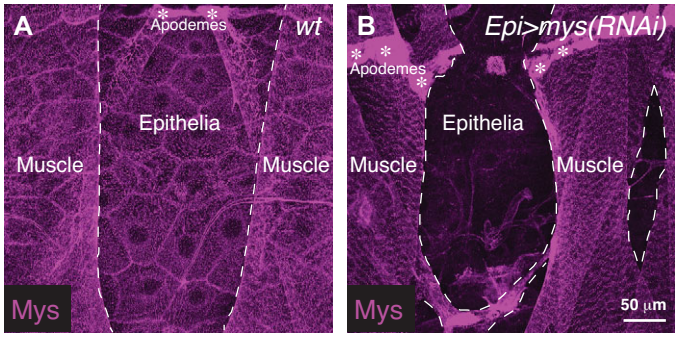

Figure S9. RNAi-mediated knockdown of epithelial Mys expression. Representative images of body wall Mys expression for wild type (A) and epithelial *mys(RNAi)* (B) are shown. Dashed white lines outline longitudinal muscles and asterisks mark apodemes. Note that epithelial *mys(RNAi)* effectively attenuates Mys levels in epithelial cells, but not muscle cells or apodemes, demonstrating the specificity of the Gal4 driver.

Table S1. ban-regulated transcripts in epithelial cells.

Up-regulated in 3rd instar *ban* mutant larvae

UNIQID	NAME	Fold Change	wild type (0013-b1)	wild type (0013-b2)	wild type (0013-b3)	wild type (0020-b1)	wild type (0020-b2)	ban (0020-b3)	ban (0020-b4)
ft01431	CG14957	54.38309826	-0.926	-0.386	-1.305	-1.655	-1.224	4.91	4.527
ft02983	mtrm	41.38135366	0.45	0	-0.518		0.018	4.87	5.697
fc31822	mTerf3	19.77716515	0.024	0	-0.198	-0.505	-0.831	3.817	4.231
fc31821	mTerf3	23.59403922	0.447	0.255	0.111	-1.784	-0.868	4.124	4.632
fc24392	Bem46	13.61779775	0.1655	0.0425	-0.2765	-0.2585	-1.2325	3.7425	3.2785
fc24391	Bem46	11.22019386	0.072	-0.127	-0.659	-0.122	-0.928	3.364	2.974
fc25516	CG8397	7.832427306	-0.8235	-0.7635	-0.7965	-0.4815	-0.6355	2.4775	2.0395
fc13695	CG14957	10.28335014	-0.805	-0.502	-0.958	0.192	0.038	3.276	2.725
ft09425	CG40002	13.98774469	-0.3715	-0.8865	-2.0935	-2.2515	-2.4645	2.2875	2.5775
fc00390	Pimet	13.43206545	0.5865	0.2905	-0.7045	-1.0885		3.3755	3.5795
fc29246	CG4570	9.002184093	-1.439	-1.888	-1.077		-1.374	1.854	2.051
ft08658	SC35	8.064435428	-0.304	0.228	-0.384	-0.534	-0.688	2.94	2.438
fc02453	grp	10.59343156	0.295	0.504	-1.001	-0.445	-1.148	3.173	3.222
fc24731	CG4594	10.68938941	0.554	0.419	0.326	-0.259	-0.875	2.972	3.946
ft05917	spn-E	10.22992091	0.4435	-0.2835	-0.1695	-0.0365	-0.7115	3.7355	2.5195
fc13376	CG4702	15.42497591	-0.357	0.511	-0.161	-0.018	-2.607	3.802	3.619
fc12616	PGRP-SA	13.40199442	-0.095	0.225	0.174	-1.422	-1.643	3.823	2.786
fc12617	PGRP-SA	14.21845636	0	0.296	0.207	-1.593	-1.786	3.933	2.906
fc31682	Ady43A	7.927964382	-0.548	-0.44	0.199	-0.784	-1.157	2.344	2.663
fc30581	Papst2	6.120105738	-0.958	-0.962	-1.334	-0.598	-1.18	1.692	1.563

Down-regulated in 3rd instar *ban* mutant larvae

UNIQID	NAME	Fold Change	wild type (0013-b1)	wild type (0013-b2)	wild type (0013-b3)	wild type (0020-b1)	wild type (0020-b2)	ban (0020-b3)	ban (0020-b4)
ft08217	Cyp4p2	0.012934911	4.111	3.925	4.629	4.643	5.013	-2.037	-1.52
ft05145	cad	0.016748094	2.6725	4.0835	2.6875	3.4785	4.0145	-2.0575	-2.8145
fc21832	CG4382	0.019567644	3.533	2.71	3.859	2.337	3.938	-1.954	-2.673
ft02746	CG14130	0.037092008	3.021	2.863	2.479	2.035	2.344	-2.942	-1.657
ft08080	CG12325	0.034088995	2.843	2.712	2.752	1.678	3.465	-1.83	-2.381
fc17436	Abl	0.066212955	1.009	1.393	1.546	1.719	1.097	-2.428	-2.66
fc03754	CG33667	0.032248651	-0.745	1.094	0.283	0.588	1.03	-4.145	-4.639
fr00526	snoRNA:Me28S-C788b	0.02076532	2.062	1.349	1.865	3.594	1.577	-4.846	-2.503
fc17435	Abl	0.062946773	0.819	1.318	1.381	1.607	0.848	-2.492	-3.095
fc21833	CG4382	0.013611545	4.582	3.77	5.095	1.825	4.022	-1.432	-2.967
fc26302	Sox102F	0.01082367	0.745	0.753	2.654	3.828		-3.251	-5.008
ft03571	CG4644	0.090373967	0.73	0.937	0.827	0.697	0.537	-2.442	-3.055
ft00305	rap	0.07176139	0.329	0.45	0.656	0.427	-0.186	-3.028	-4.018
ft07227	CG3409	0.078947074	-0.551	-0.173	0.019	-0.855	0	-3.571	-4.428
ft04329	CG8419	0.018947444	1.026	1.781	2.486	-0.745	-0.255	-4.424	-4.374
ft08088	CG30017	0.08883701	3.301	3.651	3.554	3.434	3	-0.997	0.466
ft02758	Grip163	0.042182724	1.9575	1.5485	1.4265	2.1055	3.6355	-4.0385	-1.3895
ft08218	Cyp4p1	0.012128943	2.518	1.866	0.923	2.887	-1.642	-4.187	-4.748
fc02315	CG3397	0.070869465	2.526	3.11	2.71	1.763	1.513	-1.176	-1.608
ft01633	CG15196	0.04496275	0.7745	1.6845	1.3925	2.4505	-0.1545	-3.6475	-2.5525
fc14739	Grip163	0.050937694	1.833	1.945	2.351	0.308	2.737	-1.917	-2.725
ft04133	Ucp4C	0.156783026	1.37	1.426	1.479	1.26	1.396	-1.13	-1.459
fc06063	hep	0.077451084	1.268	1.494	1.452	2.043	2.853	-1.999	-1.523
ft07069	CG31005	0.043455668	0.293	0.024	-0.442	2.152	1.047	-4.511	-3.046
fc06062	hep	0.093728032	1.621	1.803	1.861	2.404	2.896	-1.316	-1.126
ft09260	CG15400	0.10277636	-0.928	0.167	-0.086	-0.171	-0.186	-3.115	-3.972
ft05448	Crc	0.039040173	3.605	3.46	3.55	3.614	0.928	-2.454	-0.778
ft01119	CG30421	0.049349053	0.933	1.166	0	1.78		-3.507	-3.43
ft01748	sno	0.024643295	0.959	1.732	1.353		-2.074	-5.149	-4.029
fc03453	CG17568	0.048481514	-0.2445		-0.1635	1.0845	-0.0005	-4.1305	-4.5625
fc15527	Ir76a	0.027653221	2.7665	2.3435	3.9235	0.2465	1.1695	-2.0825	-3.3055
fc27070	CG9776	0.179058477	1.8765	1.9005	1.8515	1.8355	1.9335	-0.4625	-0.7555
fc20820	CG40244	0.010388539	-0.245	0.177	0.202	1.497	4.35	-4.062	-4.334
fc26243	slim	0.098689757	0.1835	-0.0245	1.0225	0.1945	1.1475	-2.3515	-3.3145
fc18150	sno	0.097995896	0.47	0.851	0.85		-0.242	-3.055	-2.853
ft03261	CG1529	0.035237435	1.7135	2.3955	2.7965	5.0575	2.7935	-0.5035	-3.6435
ft08475	CG31998	0.081798552	0.5825	1.7735	1.9395			-1.9975	-2.9125
ft02607	HGTX	0.027263781	1.67	3.241	1.161	-0.055	-0.431	-2.906	-4.4
fc01267	CG31469	0.014542143	0.503	0.13	0.145		4.186	-4.426	-3.475
fc20245	CG12065	0.114974181	0.337	1.099	0.864	0.208	0	-2.197	-3.043
fc03789	Tango6	0.070757702	1.771	2.01	2.479	3.337	3.339	-3.844	-0.199
ft06583	CG5794	0.111658002	2.114		2.865	2.429	2.151	-0.179	-1.985
ft04979	kel	0.15798186	0.7005	0.6715	0.9025	0.9405	1.2995	-1.8585	-1.6325
ft06594	CG13631	0.099913702	-0.487	-0.168	0.05	-0.05	1.076	-2.758	-3.635
fc32525	Cp7Fb	0.02045096	-0.034	0.6	1.659		4.197	-3.483	-2.947
fc02314	CG3397	0.068410779	2.353	2.903	2.57	1.765	0.56	-1.439	-1.881
ft08287	Cyp4e2	0.055960448	-0.719	-0.043	0.931	-0.362	1.852	-3.5	-3.509
fc27069	CG9776	0.176973115	1.59	1.639	1.558	1.885	1.873	-0.611	-0.977
fc10722	Obp57e	0.060088032		1.798	1.02		-0.898		-4.477
fc05719	Hsc70-2	0.021612465	2.27	2.771	3.261	4.677		-1.734	-3.158
fc16288	CG5794	0.143580054	2.429	2.441	2.926	2.709	2.448	0.278	-0.905
ft07164	CG17994	0.075834157	0.952	1.939	1.886	0.077		-1.452	-3.818
fc20244	CG12065	0.129118399	0.2815	0.9795	0.7035	-0.0275	0.0105	-2.2185	-2.8725
ft03054	RNaseX25	0.144217243	0.37	0.102	0.193	0.008	0.91	-2.696	-2.221
ft06749	scrib	0.108149673	3.768	4.256	4.214	4.325	4.581	-1.11	1.871
ft07931	Sin3A	0.095839888	0.34	-0.028	-0.326	1.272	1.15	-2.607	-2.941
ft00510	mys	0.091910806	1.529	1.355	2.007	0.49	0.312	-1.707	-2.848
fc05897	plexA	0.046323452	1.92	2.064	1.055	2.489	4.288	-1.355	-1.937
fc17672	tkv	0.135622406	1.352	1.716	1.122	1.876	1.518	-0.813	-2.184
ft03099	CG8596	0.095171726	0.723	0.713	1.99	2.243	1.793	-1.521	-2.058
fc03755	CG33667	0.061472178	-0.966	0.252	0.155	-1.629	1.034	-3.895	-4.051
fc31265	Imp	0.123685737	1.056	2.007	1.506	2.126	2.323	-0.825	-1.551
fc09500	S1P	0.08517687	0.793	0.688	1.277	1.474	2.708	-1.718	-2.253
fc32371	ssp3	0.168561006	1.025	1.241	1.094	1.359	0.906	-1.098	-1.875
fc28724	CG13875	0.083270432	1.4655	1.2545	1.3285	3.1805	2.0055	-3.0655	-0.8075

ft03236	slgA	0.088052903	0.665	0.838	0.607	2.482	1.573	-2.648	-1.669
ft08590	NijA	0.132144517	1.133	1.412	1.295	0.996	0.255	-2.449	-1.428
ft06577	CG6643	0.015425351	1.0485	0.5805	0.5215	0.3055	4.6665	-3.7015	-3.0795
ft00555	Corp	0.061488273	0.316	0.454	-2.335	0.154	-0.304	-3.648	-4.768
fc18151	sno	0.14575905	0.34	0.562	0.36	-0.34	0.361	-2.026	-3.183
fc16553	scrib	0.116822275	3.1	3.511	3.423	3.467	2.839	-2.645	1.088
ft07689	dup	0.128225639	-1.037	-0.415	-0.59	0.237	0.119	-2.849	-3.739
fc30028	ERR	0.080795735	0.228	0.116	0.589	2.091	1.811	-2.406	-2.443
fc13121	CG30438	0.175254878	0.6115	0.3955	0.7245	0.2485	0.0155	-1.8655	-2.3595
ft00803	CG4386	0.010980197	3.395	3.286	3.638	5.109	-1.415	-2.375	-3.263
fc03597	ppk6	0.083523396	1.805	2.543	1.854	0.307		-1.306	-3.013
ft05356	Mkk4	0.120219712	0.0025	0.4675	1.3625	0.6285	-0.0025	-1.8735	-3.5105
ft01398	Atg2	0.113662268	0.501	0.52	0.712	2.06	0.517	-2.162	-2.088
ft09402	eIF-4B	0.022793262	1.214	1.209	0.787	-2.554	2.646	-4.331	-3.902
fc23410	Cp1	0.086046054	0.726	0.942	1.143		2.851	-1.413	-2.877
fc05896	plexA	0.073567498	2.0955	2.2415	1.3015	2.4415	4.0575	-0.7325	-1.3755
ft06750	CG6490	0.116435078	0.7815	0.3775	1.0055	2.1325	1.3595	-2.3315	-1.4775
ft01163	gsb-n	0.024849994	2.443	2.113	4.316	0.474	-0.138	-2.829	-2.497
ft03114	Cpr65Ec	0.126890937	0.42	1.917	0.996	1.757	1.603	-1.461	-1.629
ft08342	CG30377	0.087536563	2.052	2.137	2.506	4.199	3.232	-0.522	-0.37
ft06004	Abd-B	0.060394391	0.492	1.667	0.042	2.587	2.708	-2.06	-2.331
ft05165	tadr	0.105343199	-0.103	-0.218	-0.229	-1.452	-1.668	-4.829	-3.253
fc12608	Sin3A	0.149982369	0.4035	0.6005	0.5685	0.6585	1.4055	-1.4455	-2.7785
ft03690	CG5585	0.13938445	1.533	1.527	0.815	0.456	0.594	-1.366	-2.375
fc21987	CG32043	0.133108973	1.594	1.787	2.328	2.884	2.139	-0.074	-1.789
ft06022	m-cup	0.117019094	-0.136	0.667	0.75	1.746	0.998	-1.607	-3.085
ft01052	enok	0.178197679	0.587	0.593	1.29	0.886	1.015	-1.267	-2.005
ft08752	CG33993	0.13001149	3.391	3.369	4.149	3.784	4.041	-2.462	1.764
fc32483	CG12340	0.154940793	0.036	-0.012	0.489	1.16	0.48	-2.014	-2.401
ft03749	CG7611	0.029581463	1.528	2.396	3.558		-1.221	-2.867	-2.907
fc04798	dream	0.205512178	-0.314	0.118	-0.122	0.181	0.14	-2.435	-2.122
fc29444	kuk	0.083183766	-0.1335	1.7765	2.3465	0.4105	1.4265	-1.9255	-2.4425
fc18444	CG32676	0.087946114	0.867	1.558		2.496	-0.153	-1.92	-2.192
fc20821	CG40244	0.019653282	-0.034	0.212	0.352	1.845	4.479	-2.772	-3.574
fc12416	topi	0.162256757	0.933	0.675	1.012	0.744	-0.103	-1.588	-2.359
ft04646	CG6792	0.074455263	0.271	-0.154	0.824	1.465	-1.507	-3.26	-3.269
fc03150	CG40337	0.08327479	1.064	1.406	2.099	3.251	0.713	-1.806	-1.372
fc11154	CG33272	0.025079144	1.779	2.327	2.683	0.104	5.156	-1.647	-2.334

Table S2. Genotypes used in this study.

	Panel	Label	X-chromosome	Chromosome II	Chromosome III
Figure 1	A	wt	w^{118}, *arm::GFP*^{wee}		
	A	*ban*	w^{118}, *arm::GFP*^{wee}		$ban^{\Delta}{}^{1}$/ $ban^{\Delta}{}^{1}$
	D	wt	w^{118}		
	D	*ban*	w^{118}		$ban^{\Delta}{}^{1}$/ $ban^{\Delta}{}^{1}$
	D	*UAS-ban*	w^{118}	*UAS-ban/+*	*A58-Gal4*
	E	wt	*hs-flp*^{122}	*Act-Frt-Stop-Frt-Gal4, UAS-tdTomato/+*	
Figure 2	A-I, J, K	wt	w^{118}		
	I-K	*ban*	w^{118}		$ban^{\Delta}{}^{1}$/ $ban^{\Delta}{}^{1}$
	J, K	*dup*	w^{118}	dup^{k03308}/dup^{k03308}	
	J, K	*rap*	w^{118}, rap^{G0418}		
	J, K	*UAS-ban*	w^{118}	*UAS-ban/+*	*A58-Gal4/+*
	J, K	*UAS-dm*	w^{118}	*UAS-dm/+*	*A58-Gal4/+*
Figure 3	A, G, H-J	wt	w^{118}, *ppk-3x-mCD8-GFP*		
	B, G	*ban*	w^{118}, *ppk-3x-mCD8-GFP*		
	C, G	*dup*	w^{118}, *ppk-3x-mCD8-GFP*		
	D, G	*UAS-CycE*	w^{118}, *ppk-3x-mCD8-GFP*	*UAS-CycE/+*	*A58-Gal4/+*
	E, G	*UAS-ban*	w^{118}, *ppk-3x-mCD8-GFP*	*UAS-ban/+*	*A58-Gal4/+*
	F, G	*UAS-dm*	w^{118}, *ppk-3x-mCD8-GFP*	*UAS-dm/+*	*A58-Gal4/+*
	G	*rap*	w^{118}, rap^{G0418}		*ppk-EGFP/ppk-EGFP*
	H	*ban/dup*	w^{118}, *ppk-3x-mCD8-GFP*	dup^{k03308}/+	$ban^{\Delta}{}^{1}$/+
	I	*dup +UAS-ban*		dup^{k03308}, *UAS-ban/* dup^{k03308}	*A58-Gal4, ppk-CD4-tdTomato/'ppk-CD4-tdTomato*
	J-K	*ban + UAS-dm*	w^{118}, *ppk-3x-mCD8-GFP*	*UAS-dm/+*	$ban^{\Delta}{}^{1}$, *A58-Gal4/* $ban^{\Delta}{}^{1}$
Figure 4	A, C, H, F, G	wt	w^{118}	*Ppk-CD4-tdTomato-T2A-sp11GFP/+*	*A58-Gal4/UAS-sp1-10GFP*
	D, F, G, I	*UAS-ban*	w^{118}	*Ppk-CD4-tdTomato-T2A-sp11GFP/UAS-ban*	*A58-Gal4/UAS-sp1-10GFP*
	E-G	*dup*	w^{118}	*Ppk-CD4-tdTomato-T2A-sp11GFP,* dup^{k03308}/dup^{k03308}	*A58-Gal4/UAS-sp1-10GFP*
Figure 5	A, B, G, H	wt	w^{118}	vkg^{G205}*(vkg::GFP)/+*	*ppk-CD4-tdTomato/ppk-CD4-tdTomato*
	C, G, H	*ban*	w^{118}	vkg^{G205}/+	$ban^{\Delta}1$, *ppk-CD4-tdTomato/*$ban^{\Delta}1$, *ppk-CD4-tdTomato*
	D, G, H	*UAS-ban*	w^{118}	vkg^{G205}/*UAS-ban*	*A58-Gal4, ppk-CD4-tdTomato/ppk-CD4-tdTomato*
	E, G, H	*dup*	w^{118}	vkg^{G205}, dup^{k03308}/ dup^{k03308}	*ppk-CD4-tdTomato/ppk-CD4-tdTomato*
	F-H	*UAS-dm*	w^{118}	vkg^{G205}/*UAS-dm*	*A58-Gal4, ppk-CD4-tdTomato/ppk-CD4-tdTomato*
Figure 6	A	wt	w^{118}, *arm::GFP*^{wee}		
	A	*ban*	w^{118}, *arm::GFP*^{wee}		$ban^{\Delta}{}^{1}$/ $ban^{\Delta}{}^{1}$
	B	wt	w^{118}		
	B	*ban*	w^{118}		$ban^{\Delta}{}^{1}$/ $ban^{\Delta}{}^{1}$
	B	*dup*	w^{118}	dup^{k03308}/dup^{k03308}	
	B	*rap*	w^{118}, rap^{G0418}		
	B	*UAS-CycE*	w^{118}	*UAS-CyclinE*	*A58-Gal4/+*

	B	*UAS-ban*	w^{1118}	*UAS-ban/+*	*A58-Gal4/+*
	B	*UAS-dm*	w^{1118}	*UAS-dm/+*	*A58-Gal4/+*
	C	wt	w^{1118}, *ppk-3x-mCD8-GFP*		
	D	*UAS-mysRNAi*	w^{1118}, *ppk-3x-mCD8-GFP*		*UAS-mysRNAi*^{HMS00043} */A58-Gal4*
	E	*UAS-ban + mysRNAi*	w^{1118}, *ppk-3x-mCD8-GFP*	*UAS-ban*	*UAS-mysRNAi*^{HMS00043} */A58-Gal4*
	F	*UAS-Integrins*	w^{1118}, *ppk-3x-mCD8-GFP*		*UAS-mys, UAS-mew*
	G	*ban + UAS-Integrins*	w^{1118}, *ppk-3x-mCD8-GFP*		*ban*^{s1}, *UAS-mys, UAS-mew/ A58-Gal4, ban*^{s1}
Figure 7	A-D	wt	w^{1118}	*ppk-CD4-tdTomato-T2A-sp11GFP/+*	*A58-Gal4/UAS-sp1-10GFP*
	E	wt	w^{1118}, *ppk-3x-mCD8-GFP*		
	F	*dup*	w^{1118}, *ppk-3x-mCD8-GFP*	*dup*^{k03308}*/dup*^{k03308}	
	G	*vkg*	w^{1118}, *ppk-3x-mCD8-GFP*	*vkg*^{01209}, *cn*^{1}*/ vkg*^{01209}, *cn*^{1}	
	H	*mysRNAi*	w^{1118}, *ppk-3x-mCD8-GFP*		*UAS-mysRNAi*^{HMS00043} */A58-Gal4*
Figure S1		wt	w^{1118}		
		ban	w^{1118}		*ban*^{s1}*/ ban*^{s1}
		UAS-ban	w^{1118}	*UAS-ban/+*	*A58-Gal4/+*
Figure S2		wt	w^{1118}	*ppk-CD4-tdTomato-T2A-sp11GFP/+*	*ppk-Gal4/UAS-sp1-10GFP*
Figure S3	A	wt	w^{1118}, *trol*^{zcl1700} *(trol::GFP)*		*ppk-CD4-tdTomato/ppk-CD4-tdTomato*
	B	*ban*	w^{1118}, *trol*^{zcl1700}		*ban*^{s}*1, ppk-CD4-tdTomato/ban*^{s}*1, ppk-CD4-tdTomato*
	C	*UAS-ban*	w^{1118}, *trol*^{zcl1700}	*UAS-ban/+*	*A58-Gal4, ppk-CD4-tdTomato/ppk-CD4-tdTomato*
	D	*UAS-dm*	w^{1118}	*UAS-dm/+*	*A58-Gal4/+*
Figure S4		wt	w^{1118}	*vkg*^{G205}*(vkg::GFP)/+*	*ppk-CD4-tdTomato/ppk-CD4-tdTomato*
Figure S5	A	wt	w^{1118}		
	B	*ban*	w^{1118}		*ban*^{s1}*/ ban*^{s1}
	C	*UAS-ban*	w^{1118}	*UAS-ban/+*	*A58-Gal4/+*
	E	*dup*	w^{1118}	*dup*^{k03308}*/dup*^{k03308}	
	E	*UAS-dm*	w^{1118}	*UAS-dm/+*	*A58-Gal4/+*
Figure S6	A	wt	w^{1118}		
	B	*ban*	w^{1118}		*ban*^{s1}*/ ban*^{s1}
	C	*UAS-ban*	w^{1118}	*UAS-ban/+*	*A58-Gal4/+*
	D	*UAS-dm*	w^{1118}	*UAS-dm/+*	*A58-Gal4/+*
Figure S7	E	wt	w^{1118}, *ppk-3x-mCD8-GFP*		
	F	*UAS-mysRNAi*	w^{1118}, *ppk-3x-mCD8-GFP*		*UAS-mysRNAi*^{HMS00043} */A58-Gal4*

Supplemental Materials and Methods

Dendrite measurements

To measure dendrite coverage, we used three indices. The coverage index represents the portion of the larval body wall covered by dendrites of a single neuron in dorsal hemisegments bounded by muscle attachment sites (apodemes; anterior/posterior boundaries), the dorsal midline (dorsal boundary) and a line connecting a neuron of interest to the corresponding neuron in the adjacent segments (ventral boundary). A dendrite that completely covers the dorsal hemisegment would have a coverage index of 1 whereas a dendrite that covered the entire dorsal hemisegment and territory of neighboring hemisegments would have a coverage index of > 1. The Invasion Index represents the portion of a dorsal hemisegment that is covered by dendrites of neurons from neighboring hemisegments. Midline occupancy represents the dendrite density at the midline and is expressed as dendrite length/unit area (μm dendrite length/1000μm^2).

Fluorescence-activated cell sorting (FACS)

Larvae were filleted in PBS and the tissue containing cells of interest was dissected away from all other tissues. Dissection time was limited to 30min per sample, and following dissection cell suspensions were prepared in 5 volumes of PBS/2x trypsin via 3 cycles of the following: triturate 10x through a 1000 microliter pipet tip, mix 5min at 1000 rpm in a 37°C microtube mixer. Cell suspensions were filtered through a 70um cell strainer and sorted on a FACSAria II (BD). GFP^+ non-autofluorescent events were sorted into RNAqueous-Micro Lysis buffer (Life Tech.) and frozen on dry ice.

RNA isolation, amplification, and microarray hybridization

RNA was isolated from FACS-sorted samples using an RNAqueous-Micro kit (Life Tech.) and DNase-treated. All RNA samples were subjected to two rounds of linear amplification using the Aminoallyl MessageAmp II kit (Life Tech.). Dye-coupled aRNA was fragmented and hybridized to custom-designed microarrays (Agilent).

Microarray design

We hybridized our samples to custom-designed 4x44k feature oligonucleotide microarrays (Agilent, Santa Clara, CA). We designed two 60-mer oligonucleotide probes for each of the 20,726 coding sequences in the annotated fly genome (release 5.2) using ArrayOligoSelector (Bozdech et al., 2003), resulting in 35,272 successful probe designs, 16,717 additional probes against alternatively spliced transcripts, and 546 probes targeting non-coding RNA (244 snoRNA, 108 tRNA, 24 snRNA, 74 rRNA, 3 miRNA, 93 other). The final probe set was filtered to remove redundant probes, overlapping probes, and those with cross hybridization potential (based on a -21.6 kcal/mol threshold, which was chosen to fit the number of probes allowed in the Agilent 4 x 44k design specification). This resulted in 33,792 probes to CDS, 8744 probes to alternatively spliced transcripts, and 546 RNA probes. In total, 43,803 probes were included in the design.

Microarray scanning, feature extraction, normalization, and filtering

Microarrays were scanned on an Axon 4000B scanner and feature information extracted in GenePix 6 (Molecular Devices). GPR files were uploaded into Acuity (Molecular Devices) and ratio normalized. Data was retrieved using quality filters for reference

channel intensity, background intensity, pixel saturation, pixel variance, feature diameter, % pixel intensity over background, and feature circularity. “Ratio of Medians” data was further filtered for 70% present data, Cy5 net median intensity > 350 across a minimum of 3 arrays, Cy3 net median intensity > 150 across a minimum of 20 arrays. Expression ratios were $\log_2$ transformed, arrays median centered, quantile normalized, and genes median centered before analysis.

References

Bozdech, Z., Zhu, J., Joachimiak, M. P., Cohen, F. E., Pulliam, B. and DeRisi, J. L. (2003). Expression profiling of the schizont and trophozoite stages of Plasmodium falciparum with a long-oligonucleotide microarray. *Genome Biol.* **4**, R9.